Journal of Luminescence 130 (2010) 1566–1571

Contents lists available at ScienceDirect

Journal of Luminescence

journal homepage: www.elsevier.com/locate/jlumin

# Efficient optical pumping of Zeeman spin levels in $Nd^{3+}$: $YVO_4$

Mikael Afzelius [a,*], Matthias U. Staudt [a], Hugues de Riedmatten [a], Nicolas Gisin [a], Olivier Guillot-Noël [b], Philippe Goldner [b], Robert Marino [b], Pierre Porcher [b], Enrico Cavalli [c], Marco Bettinelli [d]

[a] Group of Applied Physics, University of Geneva, CH-1211 Geneva 4, Switzerland
[b] Ecole Nationale Supérieure de Chimie de Paris (ENSCP), Laboratoire de Chimie de la Matière Condensée de Paris, CNRS-UMR 7574, ENSCP, 11 rue Pierre et Marie Curie 75231 Paris Cedex 05, France
[c] Dipartimento di Chimica Generale ed Inorganica, Chimica Analitica e Chimica, Fisica, Università di Parma, Viale G. P. Usberti 17/a, 43100 Parma, Italy
[d] Dipartimento Scientifico e Tecnologico, Univ. Verona Strada Le Grazie 15, 37134 Verona, Italy

ARTICLE INFO

Available online 23 December 2009

*Keywords:*
Rare-earth ions
Zeeman transitions
Branching ratio
Optical pumping

ABSTRACT

We demonstrate that Zeeman ground-state spin levels in $Nd^{3+}$: $YVO_4$ provides the possibility to create an efficient Λ- system for optical pumping experiments. The branching ratio $R$ in the Λ-system is measured experimentally via absorption spectroscopy and is compared to a theoretical model. We show that $R$ can be tuned by changing the orientation of the magnetic field. These results are applied to optical pumping experiments, where significant improvement is obtained compared to previous experiments in this system. The tunability of the branching ratio in combination with its good coherence properties and the high oscillator strength makes $Nd^{3+}$: $YVO_4$ an interesting candidate for various quantum information protocols.



## 1. Introduction

Rare-earth (RE) ion doped solids have recently gained interest in the context of quantum information processing applications, particularly as storage devices for light at the single photon level [1]. These quantum memories [2–6] have a role in future quantum networks [7], particularly in quantum repeaters [8,9] that can provide a scalable solution for long-distance quantum communication. In that context RE ion doped solids are interesting due to their long coherence times at cryogenic temperatures [10], which could provide coherent storage of single photons on long time scales.

In quantum memory schemes based on electromagnetically induced transparency (EIT) [11,12], controlled reversible inhomogenenous broadening (CRIB) [13–15] or atomic frequency combs (AFC) [16], the system is initialized by preparing the atoms in a well-defined ground state (state initialization). This is often realized by the usage of a Λ-system, which consists of two ground state levels (typically two spin levels) that are optically connected to one excited state. The state initialization (or spin polarization) is done by optically pumping atoms to the excited state via one leg of the Λ-system and then waiting for the atoms to de-excite to the ground state via the other leg of the Λ- system. The capability to perform good spin polarization, with close to 100% of the spins being transferred to one of the spin states, is crucial to all quantum memory schemes. The efficiency of the spin polarization depends on several parameters; (1) on the ground state and excited state lifetimes and (2) on the branching ratio $R$, which describes the probability of an excited ion to change spin level while decaying. Good branching ratios and long-lived ground states can be found in non-Kramers ions as praseodymium [17,18], europium [19,20], and thulium [21–23]. It has been considerably more difficult to obtain similar results in Kramers ions such as erbium [24,25] and neodymium [26], due to short-lived ground states and poor branching ratios. Yet, these Kramers ions are still interesting as candidates for quantum memories due to their long optical coherence times [27] and practical wavelengths where diode lasers can be used.

Here we demonstrate that Zeeman ground-state spin levels in $Nd^{3+}$: $YVO_4$ offers a magnetically tunable branching ratio $R$, resulting in an efficient Λ-system. The branching ratio is found experimentally by measuring the inhomogeneous absorption profile in a moderate magnetic field of 0.3 T, where the relative probabilities of the Zeeman transitions can be directly measured from the inhomogeneously broadened absorption spectrum. The branching ratio is measured for two magnetic field orientations and the results are compared to calculations based on crystal field theory and an effective spin $\tilde{S}=\frac{1}{2}$ model. Using the found branching value we experimentally demonstrate efficient spin initialization (97.5% spin polarization) by optical pumping in the Λ-system. These results are interesting in view of the good optical coherence times found in $Nd^{3+}$ : $YVO_4$ [26,27] and the recent demonstration of light storage at the single photon level in this system [6].

* Corresponding author. Tel.: +41 22 379 6841.
*E-mail address:* mikael.afzelius@unige.ch (M. Afzelius).

0022-2313/$ - see front matter © 2010 Elsevier B.V. All rights reserved.
doi:10.1016/j.jlumin.2009.12.026

## 2. Theory

We here investigate the $^4I_{9/2} \rightarrow {}^4F_{3/2}$ transition at 879 nm of $Nd^{3+}$ ions doped into a $YVO_4$ crystal. This crystal is uniaxial, and $Nd^{3+}$ ions substitute for $Y^{3+}$ ions in sites of $D_{2d}$ point symmetry. In a crystal field of this symmetry, the ground state $^4I_{9/2}$ splits into five Kramers doublets ($Z_1$ to $Z_5$) and the $^4F_{3/2}$ excited state splits into two Kramers doublets ($Y_1$ and $Y_2$). The transition we consider here is between $Z_1$ and $Y_1$, see Fig. 1. Under an applied magnetic field the ground and excited state doublets split into two spin sub-levels via a first-order Zeeman interaction. This gives rise to a four-level system with two ground levels and two excited levels, and the associated four possible transitions hereafter denoted a,b,c and d (see Fig. 1).

The calculation of the branching ratios between the different transitions is based on the electronic wavefunctions of $Nd^{3+}$ ions in $YVO_4$ obtained from the diagonalization of the free-ion and crystal-field Hamiltonians, using the parameters obtained by Guillot-Noël et al. in Ref. [28]. This calculation shows that for the $^4I_{9/2}(Z_1)$ and for the $^4F_{3/2}(Y_1)$ Kramers' doublets, the electronic wavefunctions are of the form (neglecting term and $J$-mixing):

$$\lambda_1|^4I_{9/2}, M=\pm\tfrac{1}{2}\rangle+\lambda_2|^4I_{9/2}, M=\mp\tfrac{7}{2}\rangle+\lambda_3|^4I_{9/2}, M=\pm\tfrac{9}{2}\rangle \quad (1)$$

and

$$|^4F_{3/2}, M=\pm\tfrac{3}{2}\rangle \quad (2)$$

where $M$ is the projection of the total $J$ moment and the $\lambda_i$ are complex coefficients. In a $D_{2d}$ site symmetry, for a $^{2S+1}L_J$ multiplet, the wavefunctions are a sum of states $|^{2S+1}L_J, \mu \pm 4m\rangle$ where $\mu$ is the crystal field quantum number [29] and $m$ an integer such that $-J \le \mu \pm 4m \le J$. For the $^4I_{9/2}(Z_1)$, we have $\mu = \pm\frac{1}{2}$ and for the $^4F_{3/2}(Y_1)$, $\mu = \pm\frac{3}{2}$ as can be seen from Eqs. (1) and (2). Without an external magnetic field, the states characterized by $+\mu$ and $-\mu$ are degenerate because of time reversal symmetry (Kramers' theorem).

Under an external magnetic field $\mathbf{B}_0$, the electronic Zeeman interaction Hamiltonian $H_{EZ}$ has to be added to the free ion and crystal field Hamiltonians, where $H_{EZ}$ is expressed as [30]

$$H_{EZ} = \beta\mathbf{B}_0 \cdot \sum_{i=1}^{n}(\mathbf{l}_i + g_s\mathbf{l}_i) = \beta\mathbf{B}_0 \cdot (\mathbf{L} + g_s\mathbf{S}) \quad (3)$$

Here $\beta$ is the electronic Bohr magneton, $\mathbf{l}_i$ and $\mathbf{s}_i$ are the individual orbital and spin momentum of the electrons and $\mathbf{L} = \sum_{i=1}^{n}\mathbf{l}_i$ and $\mathbf{S} = \sum_{i=1}^{n}\mathbf{s}_i$. $g_s$ is the gyromagnetic ratio of the electron spin which is equal to 2.0023. Under an external magnetic field, each Kramers' doublet split into two electronic singlets.

From the crystal field calculations, when $\mathbf{B}_0$ is parallel to the $c$-axis, the wavefunctions of the splitted levels are given by

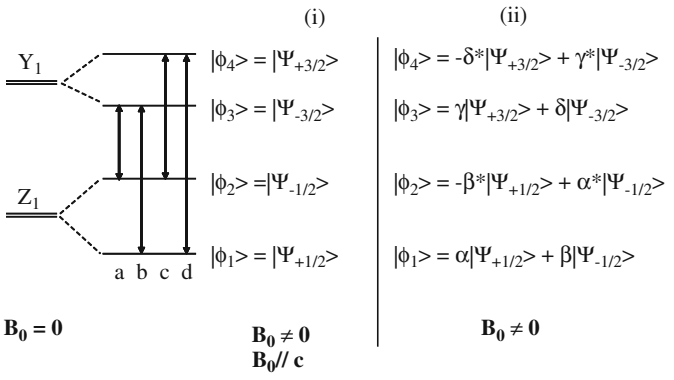


**Fig. 1.** Investigated transitions, levels and wavefunctions of $Nd^{3+}$ for a magnetic field $\mathbf{B}_0$ along the $c$-axis (i) or at an arbitrary angle $\theta$ (ii).

$|\Psi_{+1/2}\rangle$ and $|\Psi_{-1/2}\rangle$ for the lowest and the highest level of the $^4I_{9/2}(Z_1)$ doublet and by $|\Psi_{-3/2}\rangle$ and $|\Psi_{+3/2}\rangle$ for the lowest and the highest level of the $^4F_{3/2}(Y_1)$ doublet (Fig. 1 i). A general orientation of the external magnetic field $\mathbf{B}_0$, mixes the $|\Psi_{\mu}\rangle$ and $|\Psi_{-\mu}\rangle$ states and we have for the $^4I_{9/2}(Z_1)$ doublet two splitted levels $|\varphi_1\rangle$ (low energy) and $|\varphi_2\rangle$ (high energy) given by (Fig. 1 ii)

$$\begin{aligned}|\varphi_1\rangle &= \alpha|\Psi_{+1/2}\rangle + \beta|\Psi_{-1/2}\rangle \\ |\varphi_2\rangle &= -\beta^*|\Psi_{+1/2}\rangle + \alpha^*|\Psi_{-1/2}\rangle\end{aligned} \quad (4)$$

and for the $^4F_{3/2}(Y_1)$ doublet, two splitted levels $|\varphi_3\rangle$ (low energy) and $|\varphi_4\rangle$ (high energy) given by

$$\begin{aligned}|\varphi_3\rangle &= \gamma|\Psi_{+3/2}\rangle + \delta|\Psi_{-3/2}\rangle \\ |\varphi_4\rangle &= -\delta^*|\Psi_{+3/2}\rangle + \gamma^*|\Psi_{-3/2}\rangle\end{aligned} \quad (5)$$

In the following, two branching ratios will be discussed:

$$R_{\parallel} = \frac{|\langle\varphi_2|\hat{P}_{\parallel}|\varphi_3\rangle|^2}{|\langle\varphi_1|\hat{P}_{\parallel}|\varphi_3\rangle|^2} \quad (6)$$

and

$$R_{\perp} = \frac{|\langle\varphi_2|\hat{P}_{\perp}|\varphi_3\rangle|^2}{|\langle\varphi_1|\hat{P}_{\perp}|\varphi_3\rangle|^2} \quad (7)$$

where $\hat{P}_{\parallel}$ is the transition dipole operator along the $c$-axis and $\hat{P}_{\perp}$ is the operator perpendicular to the $c$-axis. If we neglect $J$-mixing, the $\Delta J = 0, \pm 1$ selection rule shows that the $^4I_{9/2}(Z_1) \rightarrow {}^4F_{3/2}(Y_1)$ transition has no magnetic dipole component. Thus, $\hat{P}_{\parallel}$ or $\hat{P}_{\perp}$ is an electric dipole operator corresponding to an electric field polarized parallel ($\mathbf{E}_{\parallel}$) or perpendicular ($\mathbf{E}_{\perp}$) to the $c$-axis. The weak $J$-mixing appearing in crystal field calculations could explain some experimental results (see Section 4.1). However, this effect is small and will not be taken into account in the following. The selection rules which hold for electric dipole transitions between the $|\Psi_{\pm\mu}\rangle$ states are

$$\langle\Psi_{\mu}|\hat{P}_{\parallel}|\Psi_{\mu'}\rangle = 0 \quad \text{unless } \mu - \mu' \text{ is even} \quad (8)$$

$$\langle\Psi_{\mu}|\hat{P}_{\perp}|\Psi_{\mu'}\rangle = 0 \quad \text{unless } \mu - \mu' \text{ is odd} \quad (9)$$

Moreover, the matrix elements for $\hat{P}_{\parallel}$ or $\hat{P}_{\perp}$ are related by

$$\langle\Psi_{\mu}|\hat{P}_{\parallel,\perp}|\Psi_{-\mu'}\rangle = -\langle\Psi_{-\mu}|\hat{P}_{\parallel,\perp}|\Psi_{\mu'}\rangle \quad (10)$$

$$\langle\Psi_{\mu}|\hat{P}_{\parallel,\perp}|\Psi_{\mu'}\rangle = \langle\Psi_{-\mu}|\hat{P}_{\parallel,\perp}|\Psi_{-\mu'}\rangle \quad (11)$$

These relations can be deduced from the symmetry properties of the electric dipole operator with respect to the crystal field and the time reversal operator [31].

The branching ratios defined in Eqs. (6) and (7) are then equal to

$$R_{\parallel} = \frac{|\alpha\gamma - \beta\delta|^2}{|\alpha^*\delta + \beta^*\gamma|^2} \quad (12)$$

and

$$R_{\perp} = \frac{|\beta\gamma + \alpha\delta|^2}{|\alpha^*\gamma - \beta^*\delta|^2} \quad (13)$$

The $\alpha$, $\beta$, $\gamma$, $\delta$ coefficients are determined by the orientation of the external magnetic field $\mathbf{B}_0$. They can be calculated directly by diagonalization of the sum of the free-ion, crystal-field and electronic Zeeman Hamiltonians or by using an effective spin-Hamiltonian model. The latter gives more accurate results when the experimental $g$-factor values are known, as is the case here. Mehta et al. [32] measured a linear Zeeman effect for magnetic fields up to 6 T. This implies that at moderate magnetic field, as

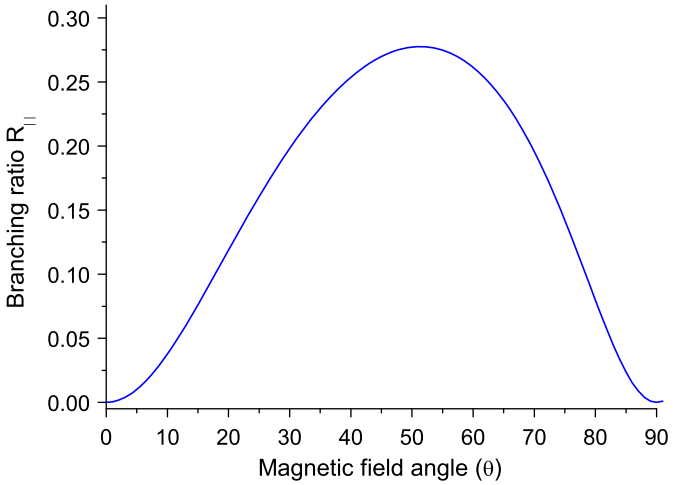


**Fig. 2.** Theoretical $R_{\parallel}$ branching ratio as a function of the angle $\theta$ between the c-axis and the magnetic field. The light is polarized along the $c$-axis ($\varphi = 0^{\circ}$).

the one we use in our experiments (0.3 T), each Kramers' doublet $Z_1$ and $Y_1$ can be described by an effective spin $\tilde{S} = \frac{1}{2}$. Quadratic splitting due to the mixing of excited Kramers' doublets with $Z_1$ and $Y_1$ are three order of magnitude smaller than the linear terms. We can thus perform a first order calculation to determine $\alpha$, $\beta$, $\gamma$, $\delta$ coefficients by diagonalization of the following spin-Hamiltonian [22,32]:

$$H_Z = \beta(\mathbf{B}_0 \cdot g \cdot \mathbf{S}) \tag{14}$$

where $g$ is the $g$-factor of the doublet under study and $\mathbf{S}$ the spin $\frac{1}{2}$ operator. Each ground and excited doublet $Z_1$ and $Y_1$ is characterized by the principal values $g_{\perp}$ and $g_{\parallel}$ of the $g$-factor since the latter is axial for a $D_{2d}$ symmetry. We used the following experimental values $^4I_{9/2}(Z_1) : |g_{\perp}| = 2.361$, $|g_{\parallel}| = 0.915$ [32]; $^4F_{3/2}(Y_1) : |g_{\perp}| = 0.28$ [26], $|g_{\parallel}| = 1.13$ [32]. To be consistent with Eqs. (4) and (5), $g$-factor values must be negative. This implies that the $M_{\tilde{S}} = -\frac{1}{2}$ spin level is equivalent to the $|\Psi_{-1/2}\rangle$ state and to the $|\Psi_{+3/2}\rangle$ state for the $^4I_{9/2}(Z_1)$ and $^4F_{3/2}(Y_1)$ doublet, respectively.

In the experiments described below, $\mathbf{B}_0$ lies in the plane containing the $c$-axis and the $\mathbf{E}$ electric field. In this case, all $\alpha$, $\beta$, $\gamma$, $\delta$ coefficients are real, so that $R_{\parallel} = 1/R_{\perp}$. A plot of $R_{\parallel}$ as a function of the magnetic field orientation is presented in Fig. 2. At $\theta = 0^{\circ}$ (i.e. $\mathbf{B}_0$ along the $c$-axis), $Nd^{3+}$ wavefunctions correspond to pure $|\Psi_{\mu}\rangle$ states (Fig. 1 i). In this case, the selection rules (Eq. (8)) show that the a and d transitions are forbidden for light polarized along the $c$-axis. Accordingly, the $R_{\parallel}$ ratio vanishes. On the other hand, when $\mathbf{B}_0$ is directed away from the $c$-axis, $Nd^{3+}$ wavefunctions are mixture of $|\Psi_{\mu}\rangle$ states and all transitions are allowed (Fig. 1 ii) until $\theta = 90^{\circ}$ where the wavefunctions are again pure $|\Psi_{\mu}\rangle$ states. $R_{\parallel}$ is predicted to reach its maximum value, $R_{\parallel} = 0.278$, for $\theta = 51^{\circ}$ (see Fig. 2). In the experiments presented in the following sections the configuration $\theta = 45^{\circ}$ was used, where $R_{\parallel} = 0.270$, close to the maximum value.

## 3. Experiment

The $YVO_4$ single crystals doped with $Nd^{3+}$ were grown by spontaneous nucleation from a $Pb_2V_2O_7$ flux [33]. Reagent grade PbO and $V_2O_5$, $Nd_2O_3$ (99.99%) and $Y_2O_3$ (99.99%) were used as starting materials in suitable amounts. The doping concentration was 0.001% (Nd/Y nominal molar ratio). The batch was put in a 50 $cm^3$ covered platinum crucible and heated to 1300 °C inside a horizontal furnace. After a soaking time of 12 h, the temperature was lowered to 850 °C at a rate of 3–4 °C/h, then the crucible was drawn out from the furnace and quickly inverted to separate the flux from the crystals grown at the bottom of the crucible. The flux was dissolved by using hot diluted nitric acid. $YVO_4$ crystallizes in the I41/amd space group, with cell parameters $a = b = 7.118$ A and $c = 6.289$ A and $Z = 4$ [34].

The crystal sample was cooled to a temperature of about 2.8 K in a pulse-tube cooler. A permanent magnetic field of 310 mT was applied along different directions. Light at a wavelength of 879 nm excited the $^4I_{9/2} \rightarrow {}^4F_{3/2}$ transition in the neodymium ions. The light pulses were created by gating an cw external cavity diode laser (Toptica DL 100) with an acousto-optic modulator (AOM), which was in a double pass configuration. Pulses of duration 10 ms were created during which the laser frequency was scanned over about 15 GHz by changing the cavity length using a piezo. After the AOM the light was split into three beams. A few percent were coupled into a Fabry–Pérot-cavity for relative frequency calibration during the scan. Another few percent were used as a reference beam for intensity normalization, which was detected by a photodiode (Thorlabs PDB150A) before the crystal. The third beam was focused onto the crystal and was detected in transmission by a second, identical photodiode. This signal was normalized by the reference signal in order to account for intensity changes during the scan. In order to control the polarization of the light incident on the crystal, a $\lambda/2$–plate was installed directly before the cooler.

## 4. Results and discussion

### 4.1. Measurement of the branching ratio

The branching ratio $R$ can be determined by measuring the absorption coefficients of the transitions a, b, c and d defined in Fig. 1. We could directly measure these by applying a relatively strong magnetic field (0.31 T), which splits the Zeeman levels sufficiently so that the different transitions could be resolved, despite the 2 GHz inhomogeneous broadening. We thus measure the transmission spectrum while scanning the laser and calculate the corresponding absorption spectrum. Note that we define the absorption depth $d$ in terms of intensity attenuation $\exp(-d)$ through the sample. In Fig. 3, we show absorption spectra taken with the magnetic field parallel $\theta = 0^{\circ}$ and at $\theta = 45^{\circ}$ to the crystal symmetry $c$-axis. In these measurements the light was polarized parallel to the $c$-axis for maximum absorption [26].

For the $\theta = 0^{\circ}$ orientation, see Fig. 3a, the b and c transitions are not resolved, but we can resolve two very weak a and d transitions at the expected positions. For this orientation we measured a branching ratio $R_{\parallel(\exp)} \approx 0.05$. Note that this value is very approximate because of the difficulty of measuring the strengths of the weak a and d transitions in Fig. 3a (particularly considering the varying background). The theoretical model predicts a branching ratio $R_{\parallel(th)} = 0$ for a magnetic field oriented along the crystal $c$-axis (see Section 2). The small contributions from the a and d transitions that are seen in Fig. 3 a could be due to a slight misalignment of the magnetic field, or due to a small magnetic dipole character for the $^4I_{9/2}(Z_1) \rightarrow {}^4F_{3/2}(Y_1)$ transition which does not vanish for this orientation. Indeed, the crystal field calculation shows that some $J$-mixing occurs in the $^4F_{3/2}$ excited state with a small contribution of the $^4F_{7/2}$ multiplet. The $^4I_{9/2}(Z_1) \rightarrow {}^4F_{7/2}$ transition with $\Delta J = -1$ has a magnetic dipole character.

For a magnetic field oriented at $\theta = 45^{\circ}$ to the crystal $c$-axis we can clearly resolve all four transitions, see Fig. 3b. Note that there is a slight intensity asymmetry in the a/d and b/c transitions, which is not expected. This is due to variations in the laser

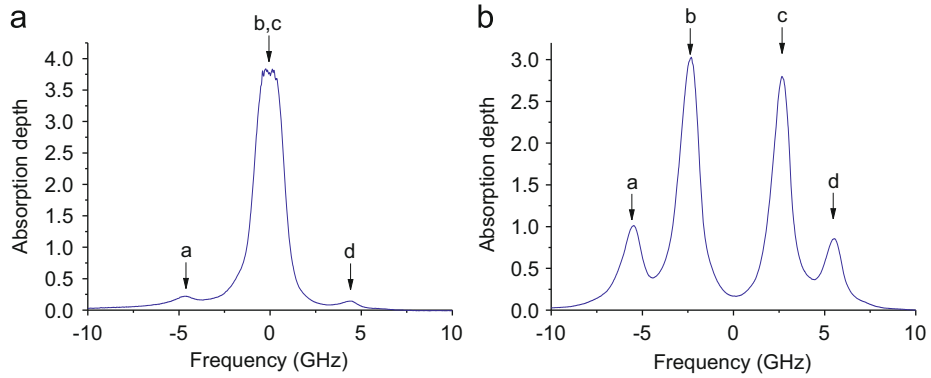


**Fig. 3.** Absorption depth as a function of frequency for a magnetic field (a) parallel $\theta = 0^\circ$ and (b) with an angle of $\theta = 45^\circ$ to the crystal c-axis. In both measurements the light polarization was chosen to be parallel to the *c*-axis. The transitions a, b, c, d are marked with the arrows.

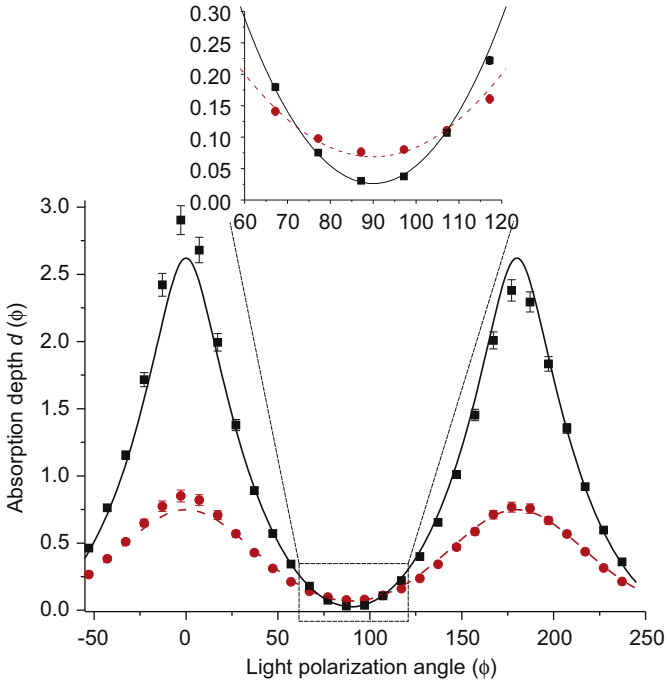


**Fig. 4.** Absorption depth $d(\varphi)$ as a function of light polarization angle $\varphi$ with respect to the crystal *c*-axis. Squares represent transitions b and c ($d_{bc}$), while circles represent transitions a and d ($d_{ad}$). We observe a clear inversion of the transition strength close to the $\varphi = 90^\circ$ orientation (see inset), as predicted by the theory (see text). The solid lines represent a fitted theoretical model explaining the variation in absorption as a function of angle. Note that the magnetic field orientation is $\theta = 45^\circ$.

intensity during the frequency scan, although most of the variation was compensated for using the reference beam (see Section 3). From this spectrum we measured a branching ratio of $R_{\parallel(\mathrm{exp})} = 0.29 \pm 0.02$ (see below on data evaluation), which is in close agreement with the theoretical value $R_{\parallel(th)} = 0.27$ (see Section 2) for a magnetic field at $\theta = 45^\circ$.

The theoretical model also predicts that the branching ratio is inverted for a polarization orientated perpendicular to the crystal *c*-axis, i.e. $R_\parallel = 1/R_\perp$. We investigated this by recording spectra while varying the light polarization angle. To extract the absorption coefficients we fit each spectrum to a simple model consisting of a sum of four Voigt functions, with (as free parameters) a common absorption depth for the b and c transitions $d_{bc}$, and for the a and d transitions $d_{ad}$. The absorption depths as a function of polarization angle are plotted in Fig. 4.

The dependence of the absorption on the polarization angle can be understood by a simple model describing the anisotropic absorption. We write the incoming field vector (at $z = 0$) as

$$\mathbf{E}_0(\varphi) = \mathbf{e}_\parallel E_\parallel(\varphi) + \mathbf{e}_\perp E_\perp(\varphi) = [\mathbf{e}_\parallel \cos(\varphi) + \mathbf{e}_\perp \sin(\varphi)]E_0 \quad (15)$$

where $\mathbf{e}_\parallel$ and $\mathbf{e}_\perp$ are unit vectors, $\varphi$ is the polarization angle with respect to the *c*-axis, and $E_0$ is the field amplitude strength at $z = 0$. The propagation of the field through the crystal is characterized by an anisotropic absorption and birefringence. It is important to note that the two orthogonal modes transform independently in the sample, due to the fact that the linear susceptibility is diagonal in the crystallographic axes for a crystal of tetragonal symmetry [35]. We can thus write the output field amplitude (at $z = L$) as

$$\mathbf{E}_L(\varphi) = [\mathbf{e}_\parallel \cos(\varphi) e^{-d_\parallel/2} + \mathbf{e}_\perp \sin(\varphi) e^{-d_\perp/2}]E_0 \quad (16)$$

where we have neglected the relative phase factor induced by the birefringence. This we can do because we have no polarization dependent optics after the sample, where only the intensity is detected

$$I_L(\varphi) = [\cos^2(\varphi)e^{-d_\parallel} + \sin^2(\varphi)e^{-d_\perp}]I_0 := e^{-d(\varphi)}I_0 \quad (17)$$

Here we have defined an effective polarization-dependent absorption depth $d(\varphi)$. We fit this formula to the experimental data in Fig. 4 (shown as solid lines), with $d_\parallel$ and $d_\perp$ as free parameters. As seen the agreement is excellent for all polarization angles. Note that the weaker a and d transitions show a sinusoidal variation, while the stronger b and c transitions deviate from a sinus due to the exponential factors in the above formula. The fitted values are $d_{\parallel ad} = 0.75 \pm 0.02$, $d_{\parallel bc} = 2.62 \pm 0.14$, $d_{\perp ad} = 0.070 \pm 0.01$ and $d_{\perp bc} = 0.025 \pm 0.01$ (all errors are those from the fit shown in Fig. 4). We can now calculate the branching ratios $R_\parallel = d_{\parallel ad}/d_{\parallel bc} = 0.29 \pm 0.02$ and $R_\perp = d_{\perp ad}/d_{\perp bc} = 2.80 \pm 1.2$. Our measurement confirms the theoretical prediction since $1/R_\perp = 0.36 \pm 0.15$ which is equal to $R_\parallel$ within the experimental errors. It should be noted, however, that the error in $R_\perp$ is probably larger than above due to systematic errors when measuring absorptions at such a low level (some percent). Nevertheless, the expect inversion in the branching ratio is clearly observed.

To conclude this section, we have shown that it possible to change the branching ratio by rotating the magnetic field with respect to the *c*-axis. While such studies have been carried out for non-Kramers ions [23], we are not aware of similar studies for Kramers ions. Our experimentally measured branching ratios at angles $\theta = 0^\circ$ and $45^\circ$ agree well with the theoretical model presented in Section 2. A more detailed and quantitative comparison would, however, require more measurements as a

function of angle. Nevertheless, our work show that a theoretical model is useful when choosing promising magnetic-field angles. Moreover, we observe experimentally the inversion of the branching ratio when changing the light polarization with respect to the *c*-axis.

### 4.2. Optical pumping

Here we will show that the $R$ value at the magnetic field orientation $\theta = 45^\circ$ makes it possible to perform efficient optical pumping. In optical pumping experiments the branching ratio must have a non-zero value ($R > 0$) in order for the ions to have a certain probability of changing spin state while decaying from the excited state. How large it must be for the optical pumping to be efficient depends on the excited state lifetime and the ground state population lifetime [25]. We here show that the branching ratio at $\theta = 45^\circ$ allows for much more efficient optical pumping than previous experiments at $\theta = 0^\circ$ [26].

The goal was to create a wide and deep transmission window within the inhomogeneous absorption profile by optical pumping. The total pump duration was 100 ms during which we made 1000 frequency sweeps over 20 MHz. The resulting absorption profile was measured in the same way as before. The probe pulses were much weaker in intensity in order not to modify the absorption during the frequency scan. From the absorption profile the percentage of ions left in the initial state could be estimated. The orientation of the polarization was $\varphi = 20^\circ$.

In Fig. 5 we show the absorption profile measured 1.3 ms after the burning pulse. This delay allowed for all ions to decay back to the ground states (the excited state lifetime being $\sim 100\,\mu s$). When optical pumping is applied (red line) a 20 MHz frequency window is created in the absorption (no pumping is represented by the black line). In Fig. 6 we show the percentage of ions left in the ground state, calculated from the absorption spectra, as a function of the delay between the end of the pump sequence and the time the scan reached the position of the bottom of the created transmission window. When extrapolating the data to zero delay we find that only 5% of the ions are left in the initial state. In terms of the total population, which is initially equally distributed over the two spin states, only 2.5% of the total

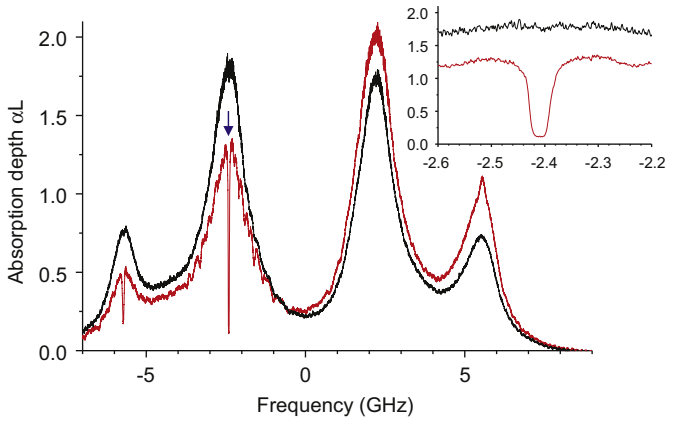


**Fig. 5.** Absorption spectra before (black line) and after (red line) optical pumping. The optical pumping creates a 20 MHz wide transmission window in the inhomogeneous absorption profile (indicated by the arrow). Note that the pumping also creates another hole in the leftmost absorption peak, since this transition starts from the same spin level. The pumped ions are moved into the two right absorption peaks, where increased absorption is observed after pumping. Inset: zoom of the created transmission window. (For interpretation of the references to color in this figure legend, the reader is referred to the web version of this article.)

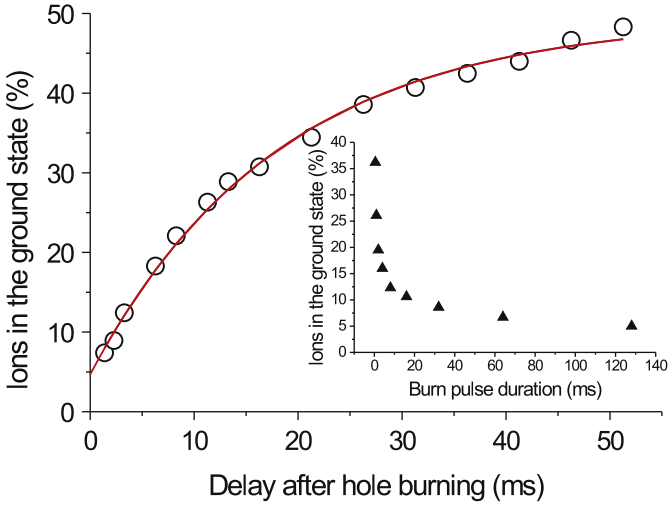


**Fig. 6.** Fraction of remaining ions in the pumped spin state as a function of the delay time after the optical pumping. The solid line is a fit with a time constant of 18 ms. Extrapolating the fit to zero delay yields about 4–5%. Inset: fraction of ions as a function of the pump pulse duration. The highest pump efficiency is obtained for pulse durations longer than 100 ms.

population is left in the initial state. This corresponds to a spin polarization of 97.5%. Note that these numbers only apply to the ions that absorb within the spectral window created. We can compare this optical pumping experiment to the one we made in a previous work [26], where we had the magnetic field oriented at $0^\circ$. In that experiment as much as 15–20% of the ions were left in the initial state (for a comparable magnetic field strength). We can thus conclude that the optimization of the branching factor $R$ improved the efficiency of the optical pumping by a factor 4–5.

From the time-resolved absorption measurement, Fig. 6, we found that about 50% of the initial absorption was recovered with a time constant of 18 ms. This decay time is given by spin population lifetime, since this decay is much longer than the excited state lifetime of 100 μs. The remaining 50% of the initial absorption recovered with a significantly slower time constant. Measurements at delay times of up to 800 ms gave a decay time of about 320 ms and at these delays the absorption tends towards the original absorption. It seems likely that this process is due to population trapping in hyperfine states of the isotopes $^{143}$Nd and $^{145}$Nd (12% and 8% natural abundances, respectively). An isotopically pure crystal would, however, be required in order to study this mechanism for population trapping. Further improvement of the optical pumping process should also be possible by higher cycling rate through stimulated emission on an auxiliary transition [25]. Stimulated emission on for example the well-known 1064 nm laser transition in Nd should decrease the excited state lifetime considerably. In addition one could force spin-mixing of the excited state Zeeman levels via radio-frequency excitation to artificially increase the branching ratio [25].

## 5. Conclusions

We have shown that $Nd^{3+}$:$YVO_4$ can provide an efficient Zeeman-level Λ-system by tuning the magnetic field orientation. The branching ratio is extracted by measuring the absorption in a moderate magnetic field where the inhomogeneously broadened Zeeman transitions can be spectrally resolved. We found that the branching ratio can be tuned by optimization of the angle between the external magnetic field and the crystal symmetry *c*-axis. We find good agreement between a theoretical model and our experimental data.

Finally we used our findings about the branching ratio in order to improve spin preparation experiments via optical pumping in this material. We created a 20 MHz wide transmission window, where only 5% of the ions were left in the initial spin state. Further improvement of the optical pumping rate should be possible with spin mixing and stimulated emission techniques.

In addition to the findings presented here it is known that neodymium shows one of the highest absorption of all rare-earth ions, a short excited state lifetime of about 100 μs [36] and good optical coherence properties [26,27]. Furthermore stable diode lasers and efficient single photon counters are available at the transition of interest in neodymium, which makes this system interesting for various quantum information and processing protocols.

## Acknowledgment

This work was supported by the Swiss NCCR Quantum Photonics, the European Commission through the integrated project QAP, and the ERC Advanced Grant QORE.

## References

[1] K. Hammerer, A.S. Sørensen, E.S. Polzik, Quantum interface between light and atomic ensemble1s, arXiv:0807.3358.
[2] B. Julsgaard, J. Sherson, J.I. Cirac, J. Fiurášek, E.S. Polzik, Nature 432 (2004) 482.
[3] T. Chanelière, D.N. Matsukevich, S.D. Jenkins, S.-Y. Lan, T.A.B. Kennedy, A. Kuzmich, Nature 438 (2005) 833.
[4] M.D. Eisaman, A. Andre, F. Massou, M. Fleischhauer, A.S. Zibrov, M.D. Lukin, Nature 438 (2005) 837.
[5] K.S. Choi, H. Deng, J. Laurat, H.J. Kimble, Nature 452 (2008) 67.
[6] H. de Riedmatten, M. Afzelius, M.U. Staudt, C. Simon, N. Gisin, Nature 456 (2008) 773.
[7] H.J. Kimble, Nature 453 (2008) 1023.
[8] H.-J. Briegel, W. Dür, J.I. Cirac, P. Zoller, Phys. Rev. Lett. 81 (1998) 5932.
[9] L.-M. Duan, M.D. Lukin, J.I. Cirac, P. Zoller, Nature 414 (2001) 413.
[10] R.M. Macfarlane, J. Lumin. 100 (2002) 1.
[11] M. Fleischhauer, M.D. Lukin, Phys. Rev. Lett. 84 (2000) 5094.
[12] M.D. Lukin, Rev. Modern Phys. 75 (2003) 457.
[13] S.A. Moiseev, S. Kröll, Phys. Rev. Lett. 87 (2001) 173601.
[14] B. Kraus, W. Tittel, N. Gisin, M. Nilsson, S. Kröll, J.I. Cirac, Phys. Rev. A 73 (2006) 020302(R).
[15] G. Hétet, J.J. Longdell, A.L. Alexander, P.K. Lam, M.J. Sellars, Phys. Rev. Lett. 100 (2008) 023601.
[16] M. Afzelius, C. Simon, H. de Riedmatten, N. Gisin, Phys. Rev. A 79 (2009) 052329.
[17] K. Holliday, M. Croci, E. Vauthey, U.P. Wild, Phys. Rev. B 47 (1993) 14741.
[18] R.W. Equall, R.L. Cone, M. Macfarlane, Phys. Rev. B 52 (1995) 3963.
[19] W.R. Babbitt, A. Lezama, T.W. Mossberg, Phys. Rev. B 39 (1989) 1987.
[20] F. Könz, Y. Sun, C.W. Thiel, R.L. Cone, R.W. Equall, R.L. Hutcheson, R.M. Macfarlane, Phys. Rev. B 68 (2003) 085109.
[21] N. Ohlsson, M. Nilsson, S. Kröll, R.K. Mohan, Opt. Lett. 28 (2003) 450.
[22] O. Guillot-Noël, Ph. Goldner, E. Antic-Fidancev, J.L. Le Gouët, Phys. Rev. B. 71 (2005) 174409.
[23] A. Louchet, Y. Le Du, F. Bretenaker, T. Channelière, F. Goldfarb, I. Lorgeré, J.L. Le Gouët, O. Guillot-Noël, Ph. Goldner, Phys. Rev. B. 77 (2008) 195110.
[24] S.R. Hastings-Simon, B. Lauritzen, M.U. Staudt, J.L.M. van Mechelen, C. Simon, H. de Riedmatten, M. Afzelius, N. Gisin, Phys. Rev. B 78 (2008) 085410.
[25] B. Lauritzen, S.R. Hastings-Simon, H. de Riedmatten, M. Afzelius, N. Gisin, Phys. Rev. A 78 (2008) 043402.
[26] S.R. Hastings-Simon, M. Afzelius, J. Minár, M.U. Staudt, B. Lauritzen, H. de Riedmatten, N. Gisin, A. Amari, A. Walther, S. Kröll, E. Cavalli, M. Bettinelli, Phys. Rev. B 77 (2008) 125111.
[27] Y. Sun, C.W. Thiel, R.L. Cone, R.W. Equall, R.L. Hutcheson, J. Lumin. 98 (2002) 281.
[28] O. Guillot-Noël, A. Kahn-Harari, B. Viana, D. Vivien, E. Antic-Fidancev, P. Porcher, J. Phys. Condens. Matter 10 (1998) 6491.
[29] K.H. Hellwege, Ann. Phys. 4 (1949) 95.
[30] B.G. Wybourne, Spectroscopic Properties of Rare Earths, Interscience, New-York, 1965.
[31] O. Guillot-Noël, et al., in preparation.
[32] V. Mehta, O. Guillet-Noël, D. Gourier, Z. Ichalalène, M. Castonguay, S. Jandl, J. Phys. Condens. Matter 12 (2000) 7149.
[33] G. Garton, S. Smith, B.M. Wanklyn, J. Crystal Growth 13–14 (1972) 588.
[34] B.C. Chakoumakos, M.M. Abraham, L.A. Boatner, J. Solid State Chem. 109 (1994) 197.
[35] R.W. Boyd, Nonlinear Optics, Academic Press, San Diego, CA, 1992.
[36] F.S. Ermeneux, C. Goutaudier, R. Moncorge, Y. Sun, R.L. Cone, E. Zannoni, E. Cavalli, M. Bettinelli, Phys. Rev. B 61 (2000) 3915.